

ENGINEERING JOURNAL

Article

Implementation and Validation of OpenFOAM for Thermal Convection of Airflow

Chakrit Suvanjumrat^{1,2}

¹ Department of Mechanical Engineering, Faculty of Engineering, Mahidol University, Nakhon Pathom 73170, Thailand

² Laboratory of Computer Mechanics for Design (LCMD), Department of Mechanical Engineering, Faculty of Engineering, Mahidol University, Nakhon Pathom 73170, Thailand

E-mail: chakrit.suv@mahidol.ac.th

Abstract. The open source code software (OpenFOAM) was applied to simulate the thermal convection of airflow. The fresh inlet airflow past a circular cylindrical heater through the variable cross-section duct by the centrifugal fan had been employed to study the thermal convection phenomenon. The widely used $k - \varepsilon$ turbulence model was implemented to simulate the thermal convection of airflow. The pressure-velocity coupling was used an effective steady state algorithm, SIMPLE algorithm, for solving a zero pressure gradient problem. The upwind differencing (UD), linear upwind differencing (LUD), QUICK, and TVD scheme were the important schemes which were selected to solve convection-diffusion problems of the airflow past a circular cylindrical heater. The thermal convection experiment was setup using the P3210 heat transfer bench of Cussons technology. The velocities of airflow had been adjusted from 5 to 20 m/s by opening a cap at the exhaust fan duct. The heater temperatures were controlled at 100, 150 and 200 °C. The computational fluid dynamics (CFD) results were compared with the experimental data. The comparison between CFD models and physical experiments were in good agreement. The average error of the $k - \varepsilon$ turbulence model by solving with the SIMPLE algorithm, UD scheme for velocity, and QUICK scheme for temperature results was less than 4.25 % when compared with the experimental data.

Keywords: Implementation, validation, OpenFOAM, convection, airflow.

ENGINEERING JOURNAL Volume 21 Issue 5

Received 30 August 2016

Accepted 21 March 2017

Published 29 September 2017

Online at <http://www.engj.org/>

DOI:10.4186/ej.2017.21.5.225

1. Introduction

The thermal convection of airflow often encountered in the baking process using the ovens. The flow past heaters were the interesting phenomenon which could apply to control the high distribution of hot airflow into the ovens [1-3]. The simulation method was popular to study the thermal convection phenomenon. The computational fluid dynamics (CFD) was the flow simulation method which reduced the expensive cost and consuming time of the trial and error method for determining the hot airflow distribution [4]. The accurate solution of the CFD method had been achieved by the appropriate flow equation. The flow behaviour inside the convection ovens preferred the turbulent flow to laminar flow caused the appearance in the flow of eddies with a wide range of length and time scales. The Reynolds-averaged Navier-Stokes (RANS) equation was used to govern the turbulent flow on the mean flow. The Reynolds stresses were the extra terms of RANS equation which happened after substituting the Navier-Stokes equation with the turbulent variables. The turbulence model was necessary to be developed for predicting and obtaining results which were close to the mean flow equation [5]. The $k - \varepsilon$ model was the two additional transport equations and the most widely used turbulence models to predict Reynolds stresses which focused on the turbulent kinetic energy effects [6-8]. Particularly, the CFD of flow simulation inside the ovens preferred to use the $k - \varepsilon$ model to other turbulence models. Many researchers used commercial CFD software such as ANSYS-Fluent, FloVent, STAR-CD, and COMSOL which had been contained the $k - \varepsilon$ turbulence model for studying and designing the good distribution of airflow [9-15]. Unfortunately, the simulated works were gathered with an expensive license cost of the commercial CFD software. There was an important obstacle for developing the convection oven of the baking process in the industrial factory. The Open Source Field Operation and Manipulation (OpenFOAM) software is under GNU General Public License without any expensive license cost. The C++ was the fundamental language which used to develop CFD codes in OpenFOAM software [16, 17]. The CFD codes had to be implemented for achievement of the precise simulation results. The flow past a cylindrical body was the basic case of approving turbulence models which similar to the flow past a heating rod of the convection oven. The specific study only airflow past a cylindrical body had been analyzed in the previous researches using the RANS equation. The variable shapes of wake vortex structure behind a circular cylinder had been observed [18-21]. This research will apply the $k - \varepsilon$ turbulence model using OpenFOAM software to study the turbulent flow past a circular cylindrical heater. The RANS equation is not adequate to solve the thermal convection problem of airflow. Consequently, the energy conservation equation will be developed in this research by using OpenFOAM codes to study the thermal convection of airflow by meaning of the temperature distribution. The RANS equation, the energy conservation equation, and the $k - \varepsilon$ turbulence model including solution methods that obtain good results in this research will be useful to analyze and design the convection oven especially the steady temperature distribution for the rubber glove baking oven in the future works.

2. Governing Equations

The turbulent flow is governed by conservation of mass, momentum, and energy equation of the mean flow [5] as follows:

$$\text{div}(\bar{U}_i) = 0 \quad (1)$$

$$\frac{\partial \bar{U}_i}{\partial t} + \text{div}(\bar{U}_i \bar{U}_j) = -\frac{1}{\bar{\rho}} \frac{\partial p}{\partial x_i} + \text{div}(\text{grad}(\bar{U}_i)) - \left(\frac{\partial (\overline{u'_i u'_j})}{\partial x_i} \right) \quad (2)$$

$$\frac{\partial \bar{T}}{\partial t} + \text{div}(\bar{T} \bar{U}_i) = \text{div} \left(\frac{1}{\bar{\rho}} \left(\frac{\mu}{P_r} \right) \text{grad}(\bar{T}) \right) - \left(\frac{\partial (\overline{u'_i T'})}{\partial x_i} \right) + \bar{S}_T \quad (3)$$

where \bar{U}_i is the time average velocity, $\bar{\rho}$ is the time average fluid density, μ is the fluid viscosity, P_r is the turbulent Prandtl number, \bar{S}_T is the source term, $-\overline{u'_i u'_j}$ is the Reynolds stresses, \bar{T} is the time average temperature, \bar{T}' is the time average temperature fluctuation.

The turbulent stresses are proportional to the mean velocity gradients or the mean rate of deformation which is written by:

$$-\overline{u_i' u_j'} = \frac{2}{3} \delta_{ij} k - \frac{\mu_t}{\rho} \left(\frac{\partial U_i}{\partial x_j} + \frac{\partial U_j}{\partial x_i} \right) \quad (4)$$

where k is turbulent kinetic energy, δ_{ij} is the Kronecker delta ($\delta_{ij}=1$ if $i = j$ and $\delta_{ij} = 0$ if $i \neq j$), ρ is the fluid density, μ_t is the turbulence viscosity.

The turbulence viscosity is given by:

$$\mu_t = \rho C_\mu \frac{k^2}{\varepsilon} \quad (5)$$

where ε is the rate of turbulent kinetic energy dissipation per unit mass, C_μ is the dimensionless constant.

The $k - \varepsilon$ turbulence model can be written as follows:

$$\frac{\partial \rho k}{\partial t} + \text{div}(\rho k \bar{U}_i) = \text{div} \left(\left(\frac{\mu_t}{\sigma_k} \right) \text{grad}(k) \right) + 2\mu_t S_{ij} \cdot S_{ij} - \rho \varepsilon \quad (6)$$

$$\frac{\partial \rho \varepsilon}{\partial t} + \text{div}(\rho \varepsilon \bar{U}_i) = \text{div} \left(\left(\frac{\mu_t}{\sigma_\varepsilon} \right) \text{grad}(\varepsilon) \right) + C_1 \frac{\varepsilon}{k} 2\mu_t S_{ij} \cdot S_{ij} - C_2 \rho \frac{\varepsilon^2}{k} \quad (7)$$

where the velocity gradient yields:

$$S_{ij} = \frac{1}{2} \left(\frac{\partial U_i}{\partial x_j} + \frac{\partial U_j}{\partial x_i} \right) \quad (8)$$

The constant variables into the $k - \varepsilon$ model are described in Table 1.

Table 1. The constant variables of the $k - \varepsilon$ model.

Constant variable	C_μ	σ_k	σ_ε	C_1	C_2
Value	0.09	1.00	1.30	1.44	1.92

3. Discretization

The transport equation of turbulence equations is generally written by:

$$\frac{\partial(\bar{\rho}\tilde{\phi})}{\partial t} + \text{div}(\bar{\rho}\tilde{\phi}\tilde{U}_i) = \text{div}(\Gamma_{\tilde{\phi}}\text{grad}(\tilde{\phi})) - \text{div}(\bar{\rho}u_i'\tilde{\phi}) + \bar{S}_{\tilde{\phi}} \quad (9)$$

where $\tilde{\phi}$ is the time average of general variables, $\bar{\rho}$ is the time average of fluid density, $\tilde{\phi}$ is the fluctuating scalar, $\Gamma_{\tilde{\phi}}$ is diffusion coefficient, $\bar{S}_{\tilde{\phi}}$ is the source term.

Discretization with the finite volume method (FVM) refers to the system of grid or cell structure as depicted by Fig. 1. The center node of the interested cell is symbolic by P . The neighbor cells around the interested cell have center nodes which symbolic by NB_i . The distance between P and NB_i is equal to Δd_i . The P cell has faces which have outer normal direction sharing around with NB_i cells.

In the steady state condition, the transient term is eliminated. The convection term, $\text{div}(\bar{\rho}\tilde{\phi}\tilde{U}_i)$, and diffusion term, $\text{div}(\Gamma \nabla \tilde{\phi})$, can be discretized using upwind differencing (UD), linear upwind differencing (LUD), the quadratic upstream interpolation for kinetics (QUICK) and the total variation diminishing (TVD) scheme which have more detail in Versteeg and Malalasekera [22]. The Reynold stresses or extra-terms, $-\bar{\rho}u_i'\tilde{\phi}$, are predicted by the $k - \varepsilon$ turbulence model which also used UD, LUD, QUICK and TVD scheme to solve the convection-diffusion term of the turbulent kinetic energy transport equation and the transport equation of rate of turbulent kinetic energy dissipation per unit mass.

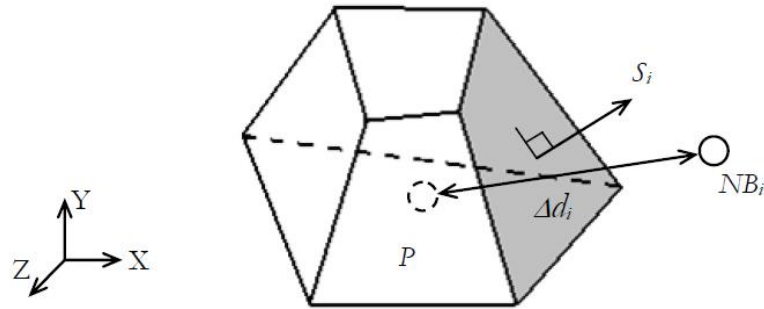


Fig. 1 The cell structure of the finite volume method.

The SIMPLE algorithm which is very good effective for the steady state problem gives a start by assuming guessed pressure into the discretized momentum equation as given by:

$$a_p u_p^* = \sum_{nb} a_{nb} u_{nb}^* - \Delta A_u (p_{i+1}^* - p_{i-1}^*) + S_\theta \Delta V_u \quad (10)$$

where a_p is the interested cell coefficient, u_p^* is the guessed velocity of an interesting velocity cell, a_{nb} is the neighbor cell coefficient, u_{nb}^* is the guessed velocity of a neighbor velocity cell, ΔA_u is the area of the velocity cells, p_{i+1}^* is the guessed pressure at a forward cell of an interesting pressure cell, p_{i-1}^* is the guessed pressure at a backward cell of an interesting pressure cell, ΔV_u is the volume of velocity cells. Notice that, the bar and tilde over parameters has been deleted to be simply for writing equations.

The guessed velocities which are solved by the previous momentum equation have been substituted into the pressure correction equation as follows:

$$a_p \hat{P}_p = \sum_{nb} a_{nb} \hat{P}_{nb} - \Delta u_p^* \quad (11)$$

where \hat{P}_p is the correction pressure of the interesting pressure cell, \hat{P}_{nb} is the correction pressure of the neighbor pressure cell, Δu_p^* is the difference of guessed velocity.

The pressure and velocity obtain from the SIMPLE algorithm using the pressure and velocity equation as given by:

$$p_p = p_p^* + \hat{P}_p \quad (12)$$

$$u_p = u_p^* + \hat{u}_p \quad (13)$$

where

$$\hat{u}_p = \frac{\Delta A_u}{a_p} \Delta \hat{P}_p \quad (14)$$

and \hat{u}_p is the correction velocity of the interesting velocity cell. The correction pressure and velocity will be close to zero after the iterative steps of the SIMPLE algorithm. The under-relaxation is necessary to use for reducing susceptibility of the divergence results. The improved pressure and velocity are obtained by:

$$p_p^{new} = p_p^* + \alpha_p \hat{P}_p \quad (15)$$

$$u_p^{new} = \alpha_u u_p + (1 - \alpha_u) u_p^{(n-1)} \quad (16)$$

where α_p is the factor of pressure under-relaxation, α_u is the velocity under-relaxation factor, $u_p^{(n-1)}$ is the previous iteration of velocity, The under-relaxation factor has values between 0 and 1.

After velocity improving, the discretized momentum equation takes the form as follows:

$$\frac{a_p}{\alpha_u} u_p^* = \sum_{nb} a_{nb} u_{nb}^* - \Delta A_u (p_{i+1}^* - p_{i-1}^*) + S_\theta \Delta V_u + \left((1 - \alpha_u) \frac{a_p}{\alpha_u} \right) u_p^{(n-1)} \quad (17)$$

Boundary condition on the cylindrical body and other walls are the no-slip condition which has form as:

$$u_p = 0 \quad (18)$$

The size of nearest cells on body surface are attempted to control by the y^+ value to support the boundary effects which has equation as written by:

$$y^+ = \frac{\Delta y_P}{\nu} \sqrt{\frac{\tau_w}{\rho}} \quad (19)$$

where y_P is the distance from the nearest cell to body surface, ν is the dynamic viscosity, τ_w is the wall shear stress, ρ is the fluid density.

The intake airflow of boundary condition is assigned by a zero gradient pressure while the uniform velocity is set up at exhaust airflow. An incompressible flow is used for air with density (ρ) and a dynamics viscosity (ν) of 1.225 kg/m³ and 1.8375×10⁻⁵ kg/(m·s), respectively. All other transport equations are solved by the SIMPLE algorithm as same as the momentum equation.

4. Experiments

The P3210 heat transfer bench of Cussons technology is employed to set up the physical experiment (Fig. 2). The heat transfer apparatus composed a square cross-section air duct which jointed with a cylindrical air duct. The square cross-section and cylindrical duct had a length of 790.00 and 1,000.00 mm, respectively. Both ducts were joined by a round to square joint with a length of 200.00 mm; therefore, the total length of the experimental duct was 1,990.00 mm. The internal dimensions of a square cross-section were height and width of 145.00 mm while an internal diameter of cylindrical duct was 145.00 mm. The square testing section was improved by installation of a circular cylindrical heater which had an external diameter of 13.00 mm. The circular cylindrical heater could adjust temperature varying from 100°C to 450 °C by a power regulator. This heater was mounted at center between paralleled gypsum plates to obstruct airflow and protect the apparatus melting. The circular cylindrical heater was set up temperatures at 100, 150 and 200°C for validation. A tangential fan was mounted at the end of a cylindrical duct which was capable to adjust air velocity rise of 30 m/s. The tangential fan inlet was connected at the end of the cylindrical duct. The fresh air would flow from an inlet of the square cross-section duct past a heater through the cylindrical duct. The exhaust air was blow out from fan outlet through the vertical duct which are controlled by the adjustable airflow speed valve (Fig. 3) for the exhaust flow velocities at 5.63, 10.47, 14.60 and 19.51 m/s to keep the Reynolds number (Re) of airflow past the heater at 4,606, 8,565, 11,944 and 15,961, respectively.

The airflow temperatures are recorded by a data logger (Hioki: model LR8431-20) through K-type thermocouple lines (Fig. 4). Two points in front of the heater (T_1 and T_2) and ten points (T_3 to T_{12}) behind were drilled in the experimental duct for measuring the airflow temperature along a center axis. The heater also uses thermocouple to measure temperature at its surface by inserting a thermocouple wire through the gypsum plate of square testing section (Fig. 4). The velocity measurement used a hot wire anemometer (Tenmars: model TM-4001). Two points (U_1 and U_2) in front of the heater and also nine points (U_3 to U_{11}) behind the heater along a center axis of the experimental duct were also specified to measure airflow speeds.

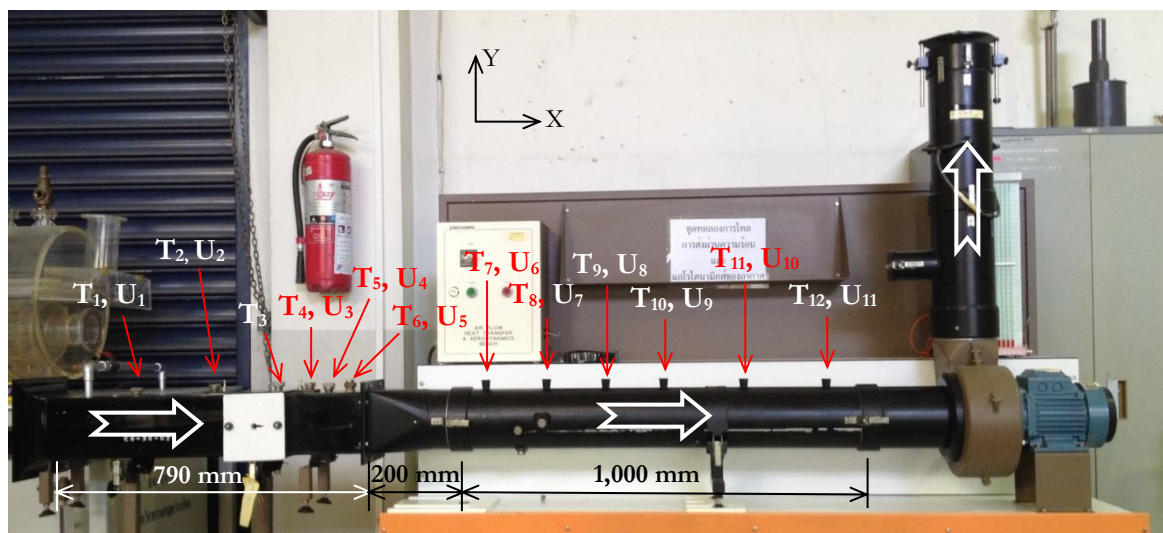


Fig. 2. The P3210 heat transfer bench. Notice that, the arrow symbol is the flow direction.



Fig. 3. The adjustable airflow speed valve.



Fig. 4. The testing section with a heater installing and temperature recording by the data logger through the K-type thermocouple wire.

5. Results and Discussion

This section would be described the experimental and simulation results of the airflow past the circular cylindrical heater. The $k - \varepsilon$ turbulence model with the different solution methods were implemented and validated with the experimental data.

5.1. Experimental Results

The airflow speeds along the center axis of the experimental duct when the adjustable airflow speed valve has been opened to keep Re of airflow past the heater at 4,606, 8,565, 11,944 and 15,961 are shown by graphs in Fig. 5. The dimensionless was used to express the measured positions of velocity along the experimental duct by referring the total duct length of 1,990.00 m. The recording data performed 30 times at each measuring point; therefore, the average, maximum, and minimum value was symbolic together and described in a legend. The airflow speeds were increased by the square to round joint which role as the nozzle. The constant speeds of airflow distinctly happened along the center axis in the cylindrical duct ($0.50 < x/L < 1.00$). The average airflow velocities were tiny fluctuating in the cylindrical duct because of the highest Re . The heater obstructed the airflow; therefore, the airflow speeds at three points were lower than other points behind the heater.

The airflow temperatures along the center axis of the experimental duct which affected by the variable Re and heater temperatures (100, 150 and 200°C) are shown by graphs in Fig. 6, 7 and 8. The heater temperatures in the airflow were swing during recording with the normal value of ± 1 °C. The measuring point (T_3) was close the heater as expected which the temperature remained airflow not heater. The temperature of inlet airflow was very affected to the temperature distribution in the cylindrical duct; therefore, the lowest temperature distribution result in the cylindrical duct obtained at the high Re. In fact, the Re had a little effect to the temperature distribution in the cylindrical duct if the fresh inlet airflow could be equivalent to the same temperature. The rising temperature of circular cylindrical heater increased the airflow temperature in the experimental duct behind the heater ($0.26 < x/L < 1.00$). On the contrary, the increase of airflow velocity reduced the airflow temperature which distinctly observed in the cylindrical duct. The thermal convection had a little effect to airflow at measuring points which was far away from the heater; therefore, the temperatures between inlet and outlet airflow at each Re were close. This experiment discovered the important effects to the thermal convection efficiency of airflow were the airflow velocity, the fresh inlet airflow temperature and the heater temperature.

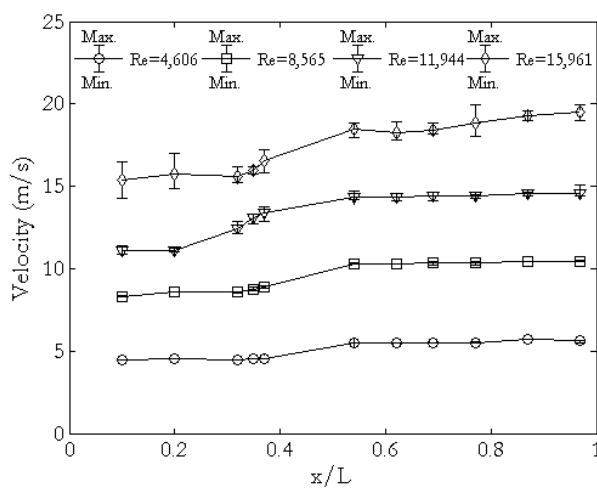


Fig. 5. The airflow speeds along a duct axis at the Re equal to 4,606, 8,565, 11,944 and 15,961.

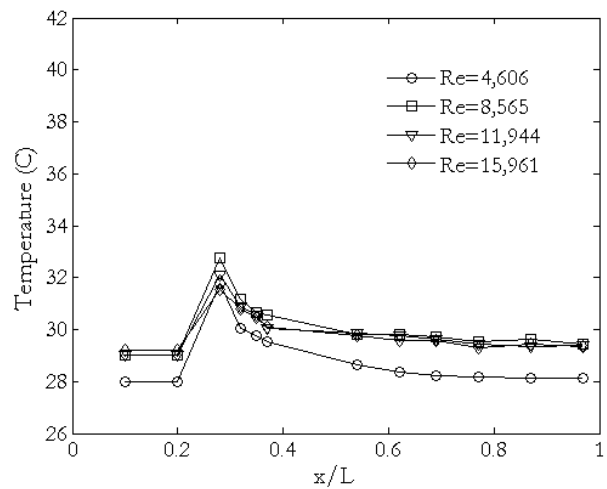


Fig. 6. The airflow temperature along a duct axis generating by the heater at 100°C.

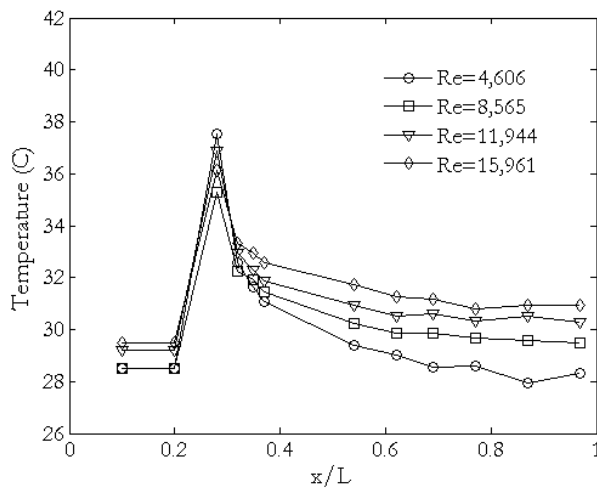


Fig. 7. The airflow temperature along a duct axis generating by the heater at 150°C.

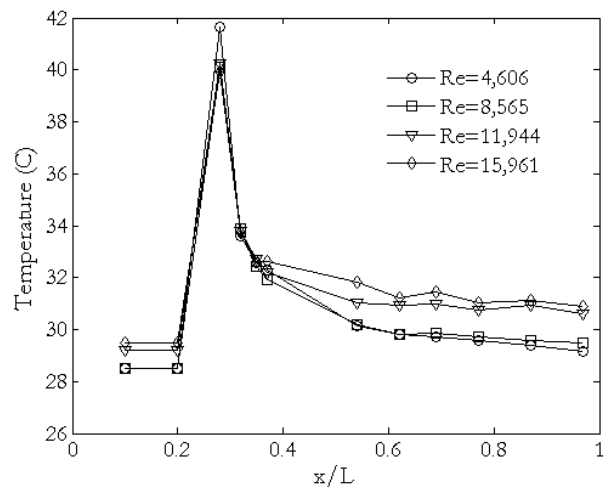


Fig. 8. The airflow temperature along a duct axis generating by the heater at 200°C.

5.2. Grid or Cell Generation

The CFD domain of the experimental duct was created by the 3D model of volumes inside the experimental duct including the square cross-section duct, the square to round joint and the cylindrical duct, respectively. The total length of the CFD domain regarding to the experimental duct was 1,990.00 mm. Figure 9 shows detail of the CFD volume that will be referred to generate the cell structure for the thermal convection simulation. The square cross-section volume was the inlet while the cylindrical volume was outlet of the airflow. The circular cylindrical heater was just modelled by a circular hole with a diameter of 13.00 mm placing across the duct volume on the Z-axis. The measured positions for velocities and temperatures of airflow were kept on the duct axis and distance from the left edge regarding to drilled holes of the experimental duct. The measuring positions (X,Y,Z) are described in Fig.9. The original point (X=0, Y=0, Z=0) was placed on the center of the inlet surface on the square cross-section duct side.

The CFD volume was divided by the 3D unstructured cells (tetrahedrons).The finest unstructured cells are generated around the surface of circular cylindrical heater for keeping y^+ values lower than +11.63 [23] which takes the near-wall flow to be laminar (Fig. 10). The average y^+ value on the heater surface was +9.43. The cell independence was performed by increasing cells inside the CFD volume until the airflow temperature of CFD results was given a constant value. The CFD results depending on the number of cells are plotted by graph as shown in Fig. 11. The number of cells which was optimum to simulate by CFD method was selected by using graphs in Fig. 11. The constant temperature of two simulating points happened at 428,239 cells and then there were the appropriated cells for implementation and validation of the CFD codes. Figure 12 shows the final cell structure of the airflow past the heater of the heat transfer bench. The convection volume where was around the circular cylinder heater were filled with the finest cells.

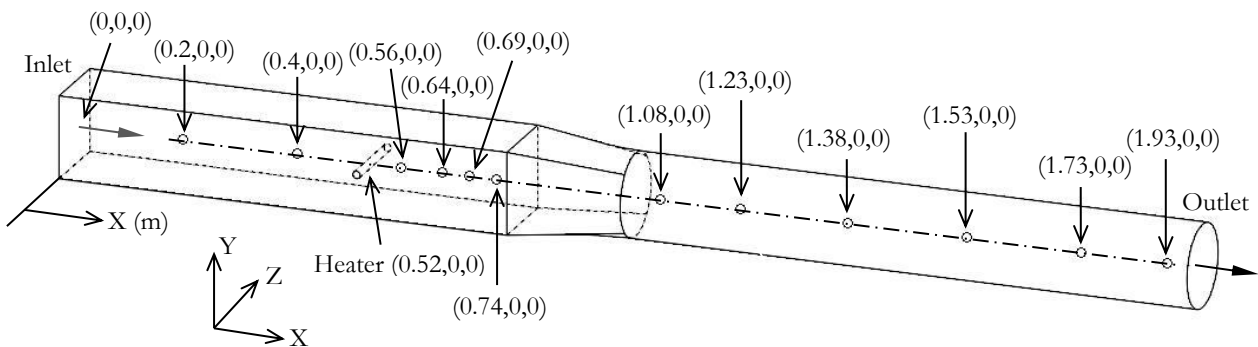


Fig. 9. Description of the CFD volume for the thermal convection of airflow simulation.

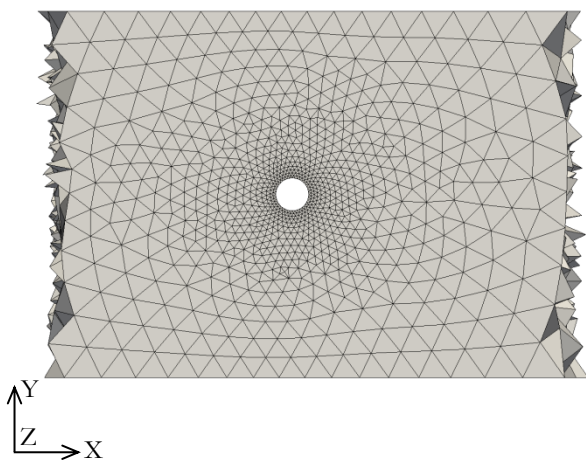


Fig. 10. The finest cells around the circular cylinder heater.

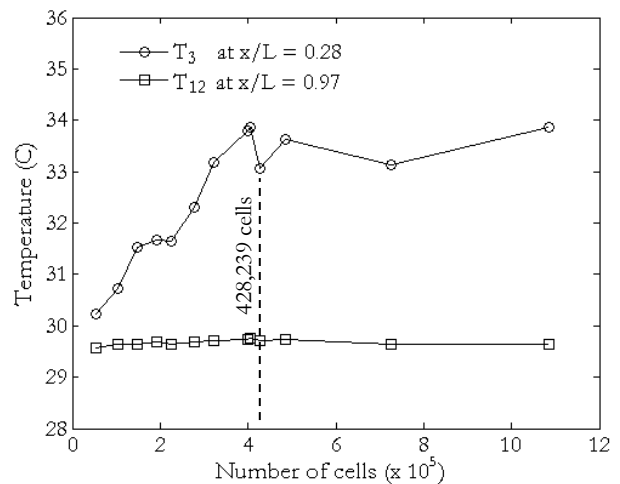


Fig. 11. The CFD temperature at T_3 and T_{12} point correlating to variable numbers of cells.

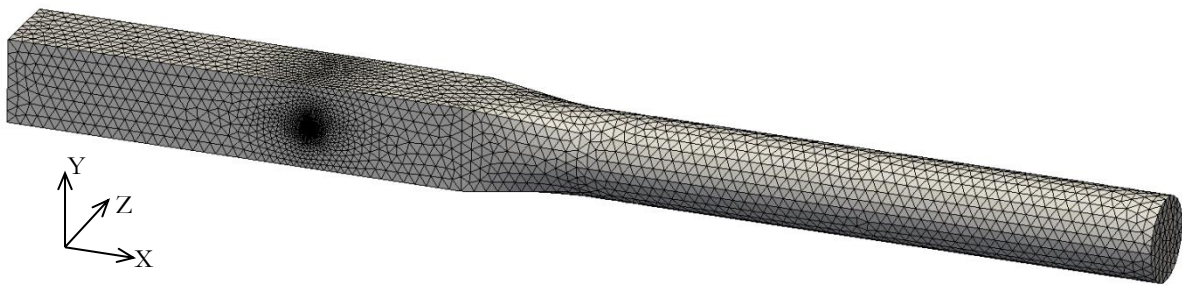


Fig. 12. The final cell structure for the thermal convection of airflow simulation.

The inlet temperature and outlet velocity of airflow would assign regarding to each experiment data for implementing and validating the CFD codes. The temperature of heater was assign on the circular cylinder surface using the average temperature of the experimental data (100, 150 and 200 °C). The outer surfaces of cell structure were assigned by wall conditions comprising no-slip and adiabatic wall. Notice that, the personal computer with Core i5 CPU and 4 GB DDR2 SDRAM memory was used to perform all of CFD models.

5.3. CFD Results

The simulation of airflow past a circular cylindrical heater inside duct had been performed using $k - \varepsilon$ turbulence model. The SIMPLE algorithm and UD scheme were used to solve this CFD model based on the steady state condition. The variable speeds of airflow along the duct axis by the CFD simulation and physical experiment are compared by graphs as shown in Fig. 13. Notice that, the LUD, QUICK and TVD had divergent velocity results under whole conditions as same as the UD scheme. The $k - \varepsilon$ turbulence model which solved by the UD scheme had trend of graphs were in a very good agreement with experimental data. The airflow velocities nearly inlet and outlet surface of CFD results were very close to the experimental data. The distance behind the circular cylindrical heater ($0.26 < x/L < 0.40$) was extremely affected to increase errors of the airflow simulation results (U_3 , U_4 and U_5) by the obstruction more than any area along the axis of cell structure. Another interesting area was near a tip of the nozzle (the square to round joint) that the CFD results were over estimate than the experimental data. The high velocity of the exhaust airflow induced error increasing at these areas. The comparison expressed the UD scheme obtained absolute average error of 4.31, 5.87, 5.96 and 6.05% along the variable cross-section duct at Re of 4,606, 8,565, 11,944 and 15,956, respectively. The error increasing regarded to the increase of turbulent flow. This effect might cause the cell numbers which were not proper for the higher Re.

Figure 14 shows the streamlines of airflow through the duct using the UD scheme. The colors mean the velocity of airflow was the maximum value when the streamlines were in red and the minimum value when the streamlines were in blue. The red streamlines happened inside the cylindrical duct at the Re was equal to 15,956. The airflow velocity above the heater surface increased from velocity at the inlet surface caused the gap between the heater and the upper of duct wall was less than the square cross-section area of the inlet side duct. Consequently, there was the area reducing which shape as similar as the nozzle. The airflow velocity below the heater surface also increased with the same reason.

Figure 15 shows the streamlines behind the heater at Re equal to 4,606 and 15,959. The streamlines were distinctly turbulent backward the heater surface. It was also found that the velocity of airflow nearly the surface backward the heater was less than other areas on the heater surface. This separated flow phenomenon occurred by the obstacle object. The smooth streamlines of airflow left the turbulent phenomenon were not over twice lengths of a heater diameter then the streamlines were smoothly illustrated again.

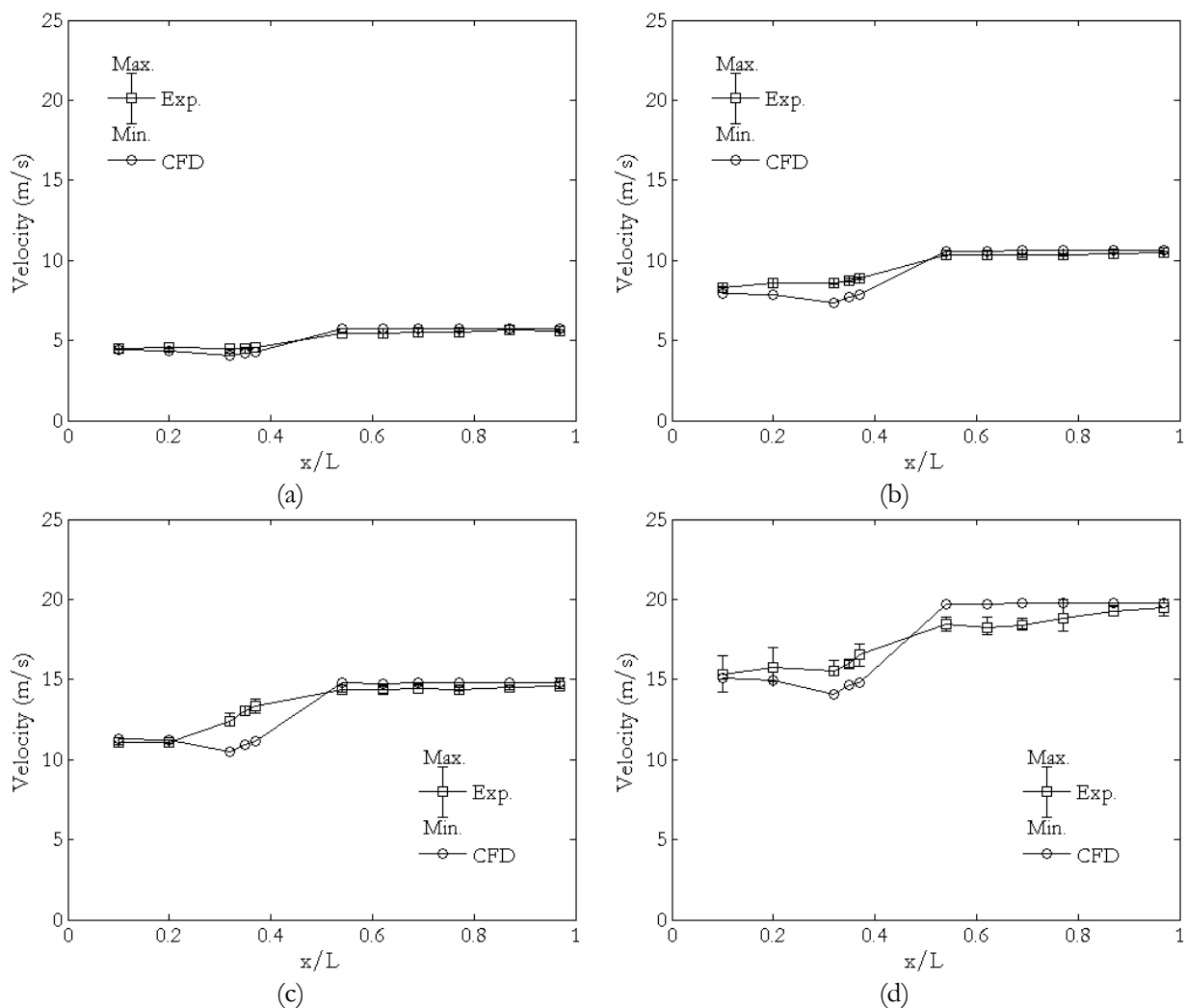


Fig. 13. The comparison of airflow velocities between CFD results and experimental data at the Re of: (a) 4,606, (b) 8,565, (c) 11,944, and (d) 15,961.

The temperatures of airflow along the duct axis at the Re of 4,606 and 8,565 are plotted by graphs as shown in Fig. 16. Figure 17 shows the comparison graphs of airflow temperatures between the CFD simulation and physical experiment at Re is equal to 11,944 and 15,956. The different schemes which were employed to solve the temperature distribution along the duct axis strongly affected to the accuracy of the CFD model. The QUICK scheme had trend of the temperature distribution along the duct axis closer experimental data than the other schemes. The airflow velocity also had a great effect to the accuracy of schemes. The temperature distribution of the CFD results was low estimate when the airflow was in the critical length behind the heater ($0.26 < x/L < 0.40$). This duct length occurred the turbulent streamline that mean the fluctuating results were recorded. The T_3 point was in the large eddy flow then it had the higher error than other points of simulation when the Re was increased. However, the QUICK scheme was the efficient scheme to solve temperatures in the critical length. The smooth streamlines length ($0.50 < x/L < 1.00$) had the constant temperature. The QUICK scheme remained the efficient scheme to solve the CFD model in this length. The temperature results of the QUICK scheme were almost synchronized with the experimental data at the heater temperature of 100 °C over all airflow velocity. The temperature distribution of the CFD results was under estimate when the airflow velocities were increased. The high velocity of airflow reduced the airflow temperatures from the critical length which were observed at the recorded temperatures in the cylindrical duct ($0.5 < x/L < 1$). The error of the solution methods (the UD and LUD scheme) was affected by the high airflow velocity. The effect might be from the false diffusion which happened by using the UD and LUD scheme to solve the diffusion-convection equation. However, all CFD results by different scheme were in a good agreement with the experimental data which

could validate OpenFOAM software to use for simulating the thermal convection of airflow inside the duct. Table 2 concludes the average error of airflow temperatures by CFD codes. The UD, LUD, QUICK and TVD scheme were obtained total average error of 3.22, 3.47, 2.95 and 3.06%, respectively. The QUICK scheme was an average error less than other schemes; therefore, it was suitable to solve the temperature distribution inside the long duct with the variable cross-section area.

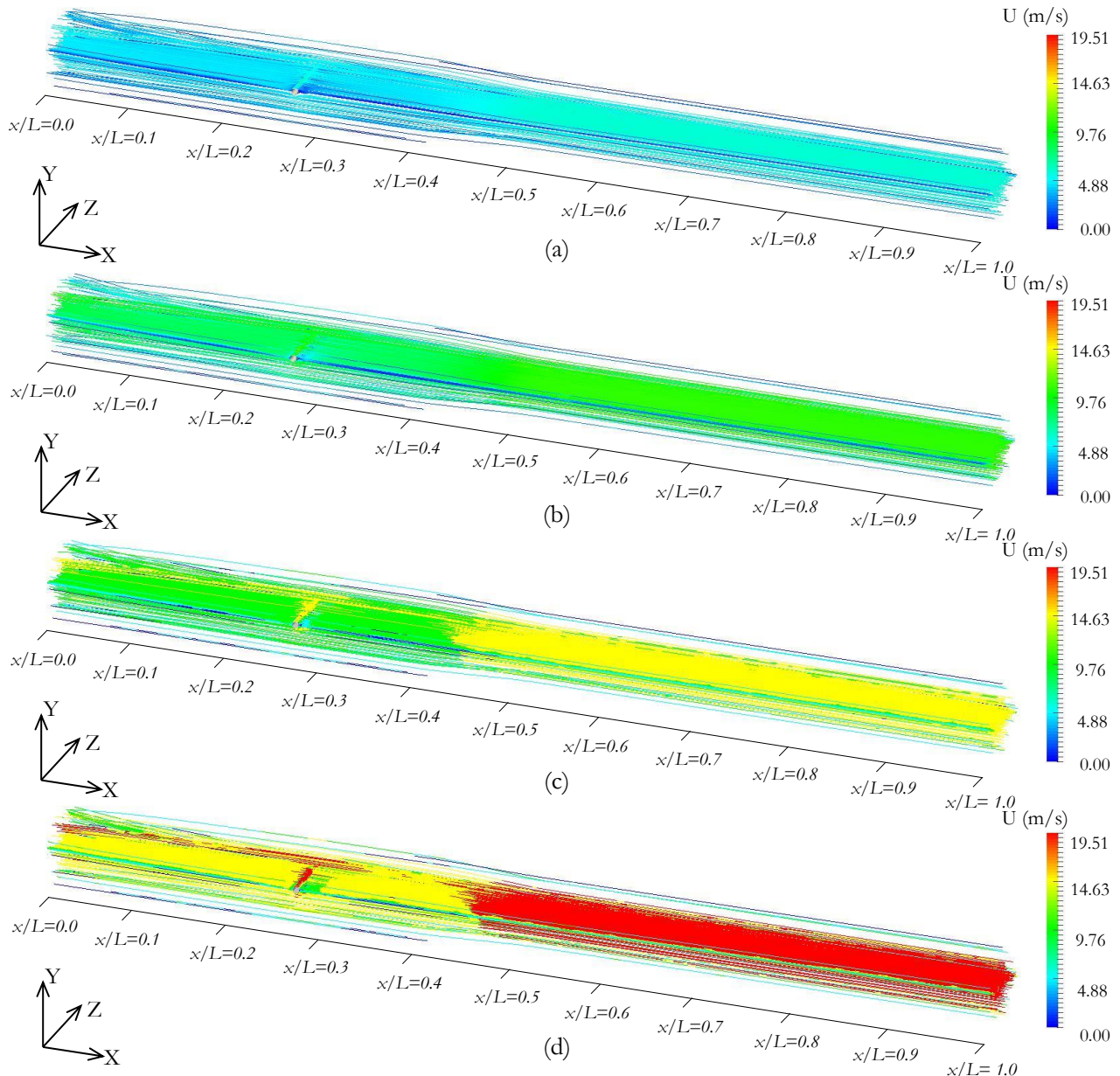


Fig. 14. The streamlines of airflow velocity inside the duct at the Re of: (a) 4,606, (b) 8,565, (c) 11,944 and (d) 15,961.

The airflow temperature distribution could illustrate by the color contour on a symmetric plane (X-Y plane) to observe the heater temperature effect. Figure 18 shows the airflow temperature distribution of the CFD model by solving with the QUICK scheme at the Re is equal to 4,606. The airflow temperature was high in the critical length and low in the smooth streamlines length inversely the airflow speeds behind the heater. The maximum temperature (red) of airflow increased regarding to temperatures of a heater. The airflow temperature was risen up backward the heater surface and extended heat distance when heater temperatures were increased. The color of temperature changed from red to blue along an axis of duct behind the heater caused of airflow velocity increasing. Figure 19 shows the airflow speed effect to the

airflow past the heater which set up a heater temperature at 200°C. The airflow speed had a lot of effects to reduce the thermal distribution. The maximum temperatures of airflow (red) backward the heater surface was shortened when the airflow speeds were increased.

Table 2. The average error of temperature results by the different solution methods.

Scheme	Temp. (°C)	The average error of schemes (%)			
		Re = 4,606	Re = 8,565	Re = 11,944	Re = 15,961
UD	100	1.66	1.71	1.63	1.08
LUD		2.16	1.98	1.78	1.27
QUICK		2.59	1.22	1.27	0.85
TVD		3.01	1.20	1.27	0.86
UD	150	2.40	2.08	4.67	5.93
LUD		2.57	2.46	4.86	6.10
QUICK		2.92	1.43	4.10	5.40
TVD		3.07	1.24	4.10	5.49
UD	200	1.87	4.09	5.34	6.17
LUD		2.08	4.51	5.56	6.36
QUICK		2.79	2.95	4.54	5.43
TVD		3.46	2.91	4.53	5.54

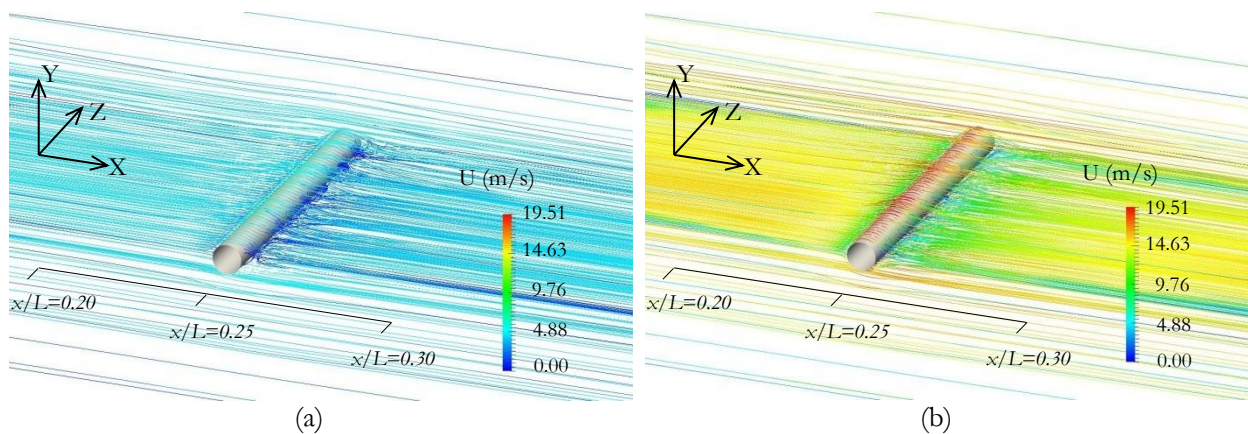


Fig. 15. The turbulent flow after airflow past the heater at the Re of: (a) 4,606 and (b) 15,961.

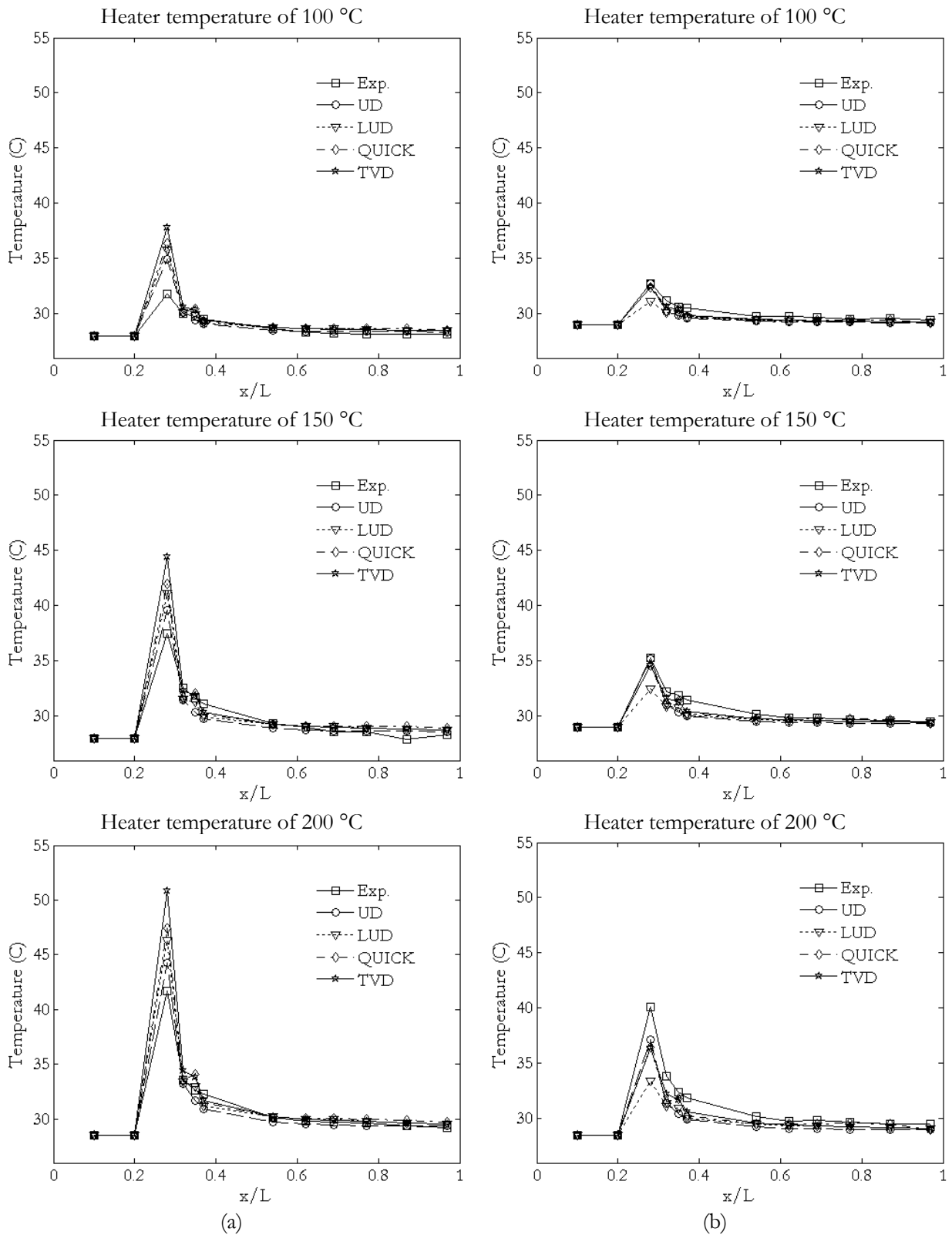


Fig. 16. The temperature distribution of airflow along duct axis at the Re of: (a) 4,606 and (b) 8,565.

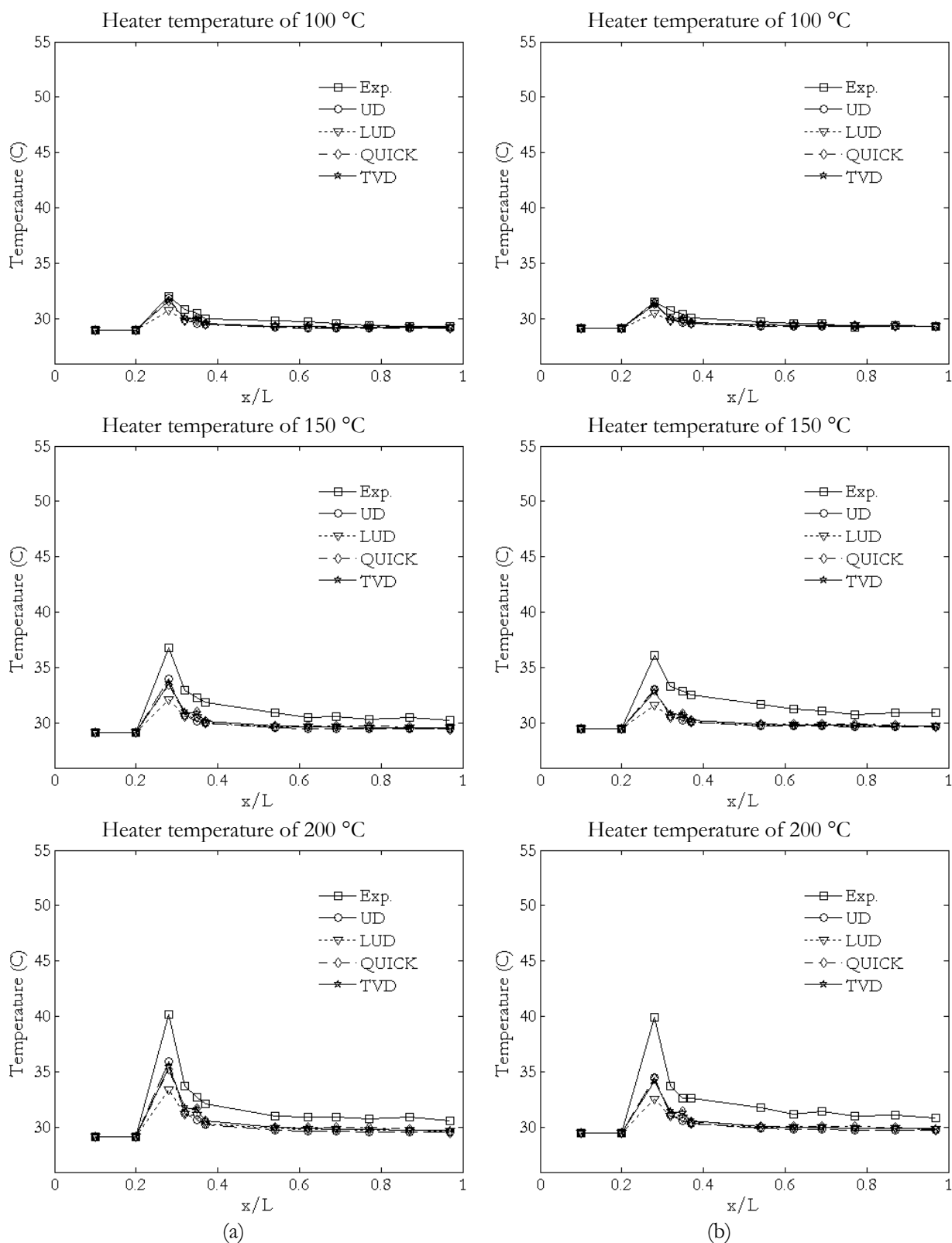


Fig. 17. The temperature distribution of air flow along duct axis at the Re of: (a) 11,944 and (b) 15,961.

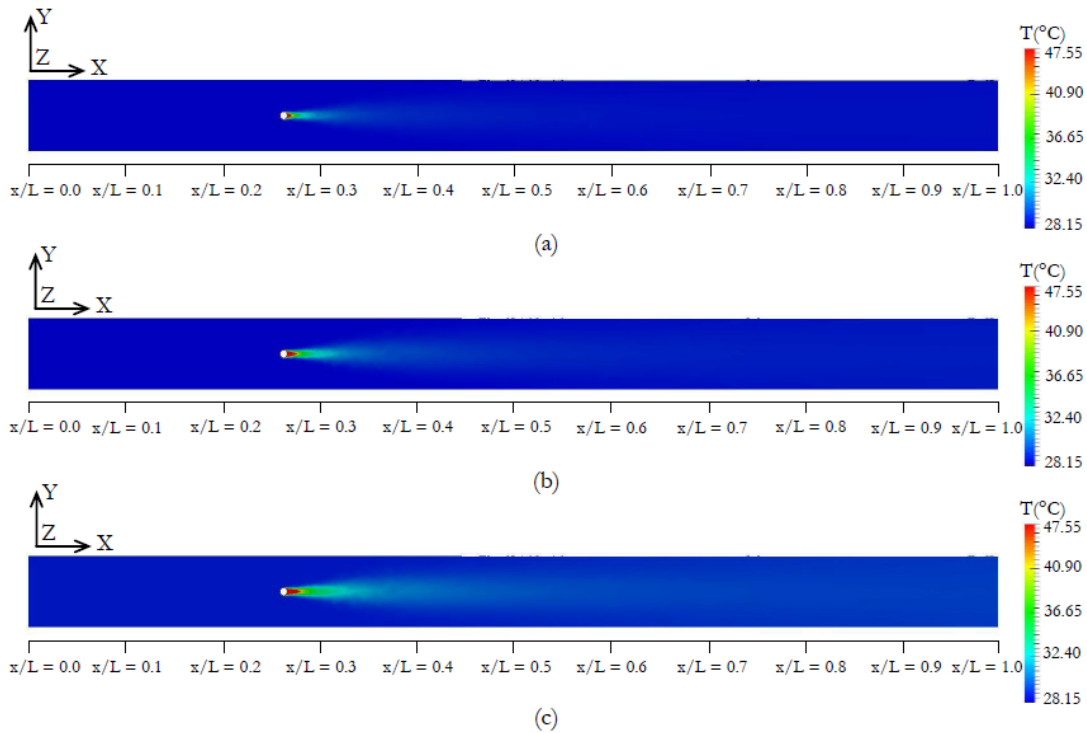


Fig. 18. The temperatures distribution of airflow inside the CFD model duct using: (a) 100°C, (b) 150°C and 200°C heater at $Re = 4,606$.

6. Conclusions

The $k - \varepsilon$ turbulence model for simulation the thermal convection of airflow inside the long duct was implemented using the open source code CFD software, OpenFOAM. The CFD domain was modelled by controlling finest tetrahedron cells around a circular cylinder heater which had distance from the heater surface to its nodes not over than the value that made y^+ more than +11.63. The average value of y^+ around the heater surface was +9.43 for keeping the near-wall flow to be laminar. The number of cells also had been controlled for the convergence of simulation results; therefore, the total 3D unstructured cells were 428,239.

The SIMPLE algorithm was chosen for the steady state simulation while four schemes composing UD, LUD, QUICK and TVD scheme were employed to determine the suitable scheme of the $k - \varepsilon$ turbulence model. The UD was the suitable scheme to solve velocities of the $k - \varepsilon$ turbulence models because it only had convergent results under the final cell structure. Meanwhile the QUICK scheme was the least average error of temperature results for the comparison with the experimental data. The accuracy of this CFD model was validated by the experimental data. The average error of CFD results which were velocity and temperature was 5.55% and 2.95%, respectively. The simulation results illustrated the streamlines were formed to be turbulent flow backward the heater, therefore, the efficient thermal convection between the heater and airflow occurred in this area as well. The airflow temperature reduction was inversely proportional to airflow velocity increase. The comparison of turbulence models and solution methods for this research were concluded that the $k - \varepsilon$ turbulence model with the SIMPLE algorithm, UD scheme to solve velocity and QUICK scheme to solve temperature was suitable for simulation thermal convection of airflow inside the long duct with the variable cross-section area. This CFD model had been validated which gave the very good agreement with the experimental data. Consequently, the CFD model in this research was recommended for using to study and design the temperature distribution in the convection oven especially the steady temperature distribution for the rubber gloves baking oven in the future work. Particularly, the OpenFOAM software is the excellent software for simulating the thermal convection of airflow inside duct without the expensive license cost.

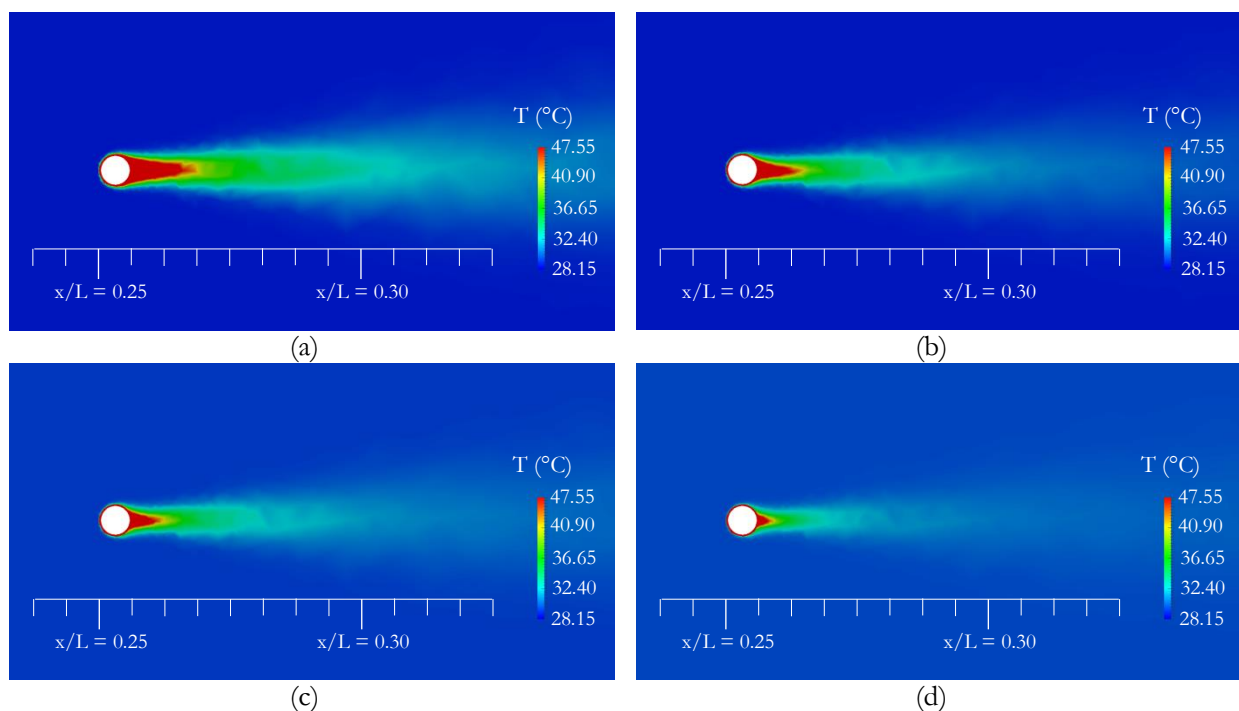


Fig. 19. The temperature distribution of airflow in the critical length after past the 200°C heater at the Re of: (a) 4,606, (b) 8,565, (c) 11,944 and (d) 15,961.

Acknowledgment

The author wishes to thank our graduate student, Mr. Kittipos Loksupapaiboon, for supporting the experimental data and simulation data in this research.

References

- [1] T. Watanabe, T. Orikasa, H. Shono, S. Koide, Y. Ando, T. Shiina, and A. Tagawa, "The influence of inhibit avoid water defect responses by heat pretreatment on hot air drying rate of spinach," *J. Food Eng.*, vol. 168, pp. 113-118, Jan. 2016.
- [2] A. C. Ma, Y. Li, and H. L. Dong, "Optimized temperature uniformity and pressure loss in the baking finish oven of the enameled wire," *Appl. Term. Eng.*, vol. 78, pp. 670-681, Mar. 2015.
- [3] J. K. Carson, J. Willix, and M. F. North, "Measurement of heat transfer coefficients within convection ovens," *J. Food Eng.*, vol. 72, no. 3, pp. 293-301, Feb. 2006.
- [4] N. Chhanwal, A. Tank, K. S. M. S. Raghavarao, and C. Anandharamakrishnan, "Computational fluid dynamics (CFD) modelling for bread baking process-a review," *Food Bioprocess Technol.*, vol. 5, no. 4, pp. 1157-1172, May. 2012.
- [5] H. K. Versteeg and W. Malalasekera, "Turbulence and its modelling," in *An Introduction to Computational Fluid Dynamics: The Finite Volume Method*, 2nd ed. Malaysia: Pearson Education Limited, 2007, ch. 3, pp. 40-114.
- [6] B. E. Launder and D. B. Spalding, "The numerical computation of turbulent flows," *Comput. Method Appl. M.*, vol. 3, no. 2, pp. 269-289, Mar. 1974.
- [7] E. Turgeon, D. Pelletier, J. Borggaard, and S. Etienne, "Application of a sensitivity equation method to the $k - \epsilon$ model of turbulence," *Optim. Eng.*, vol. 8, no. 4, pp. 341-372, Dec. 2007.
- [8] W. N. Edeling, P. Cinnella, R. P. Dwight, and H. Bijl, "Bayesian estimates of parameter in the $k - \epsilon$ turbulence model," *J. Comput. Phys.*, vol. 258, pp. 73-94, Dec. 2014.
- [9] H. Isleroglu and F. K. Ertekin, "Modelling of mass and heat transfer during cooking in steam-assisted hybrid ovens," *J. Food Eng.* vol. 181, pp. 50-58, Jul. 2016.
- [10] J. Smolka, Z. Bulinski, and A. J. Nowak, "The experimental validation of a CFD model for a heating oven with natural air circulation," *Appl. Term. Eng.*, vol. 54, no. 2, pp. 387-398, May 2013.

- [11] M.H. Ghadiri, N.L.N. Ibrahim, and M.F. Mohamed, "Performance evaluation of four-sided square wind catchers with different geometries by numerical method," *Engineering Journal*, vol. 17, no. 4, pp. 9-17, Oct. 2013.
- [12] L. Anetor, E. Osakue, and O. Odetunde, "Reduced mechanism approach of modeling premixed propane- air mixture using ANSYS Fluent," *Engineering Journal*, vol. 16, no. 1, pp. 11-22, Jan. 2012.
- [13] F. Ismail, A. I. Rashid, and M. Mahbub, "CFD analysis for optimum thermal design of a carbon nanotube based micro-channel heatsink," *Engineering Journal*, vol. 15, no. 4, pp. 11-22, Oct. 2011.
- [14] Y. Amanlou and A. Zomorodian, "Applying CFD for design a new fruit cabinet dryer," *J. Food Eng.* vol. 101, no. 1, pp. 8-15, Dec. 2010.
- [15] M. Promtong and P. Tekasakul, "CFD study of flow in natural rubber smoking-room: I. Validation with the present smoking-room," *Renew. Energy*, vol. 27, no. 11-12, pp. 2113-2121, Aug. 2007.
- [16] C. J. Greenshields, "Copyright notice," in *OpenFOAM: The Open Source CFD Toolbox(Programmer's Guide version 3.0.1)*, UK: OpenFOAM Foundation Ltd., 2015, pp. 2-6.
- [17] C. J. Greenshields, "Copyright notice," in *OpenFOAM: The Open Source CFD Toolbox(User Guide version 3.0.1)*, UK: OpenFOAM Foundation ltd., 2015, pp. 2-6.
- [18] B. Zhou, X. Wang, W. Guo, W. M. Gho, and S. K. Tan, "Control of flow past dimpled circular cylinder," *Exp. Therm. Fluid Sci.*, vol. 69 pp. 19-26, Dec. 2015.
- [19] D. Jinlong and H. Weiping, "CFD-based numerical analysis of a variable cross-section cylinder," *J. Ocean Univ. China.*, vol. 13, no. 4, pp. 584-588, Jan. 2014.
- [20] S. Singha and K. P. Sinhamahapatra, "Flow pas a circular cylinder between parallel walls at low Reynolds numbers," *Ocean Eng.*, vol. 37, no. 8-9, pp. 757-769, Jun. 2010.
- [21] P. M. Rao, K. Kuwahara, and K. Tsuboi, "Simulation of unsteady viscous flow around longitudinally oscilating circular cylinder in a uniform flow," *Appl. Math. Model.*, vol. 16, no. 1, pp. 26-35, Jan. 1992.
- [22] H. K. Versteeg and W. Malalasekera, "The finite volume method for convection-diffusion problem," in *An Introduction to Computational Fluid Dynamics: The Finite Volume Method*, 2nd ed. Malaysia: Pearson Education Limited, 2007, ch. 5, pp. 134-178.
- [23] H. K. Versteeg and W. Malalasekera, "Implementation of boundary conditions," in *An Introduction to Computational Fluid Dynamics: The Finite Volume Method*, 2nd ed. Malaysia: Pearson Education Limited, 2007, ch. 9, pp. 267-284.